ISME

Free Vibration Analysis of Thin Annular Plates Integrated with Piezoelectric Layers using Differential Quadrature Method

K. Arteshyar[*]
Graduate Student

M. M. Mohieddin Ghomshei[†]
Assistant Professor

In this article, using generalized differential quadrature (GDQ) methods, free vibration of a thin annular plate coupled with two open circuit piezoelectric layers, is numerically studied based on the classical plate theory. The governing differential equations with respective boundary conditions are derived and transformed into a set of algebraic equations by implementing the GDQ rule, then solved as an eigenvalue problem to obtain the natural frequencies and mode shapes of the plate. Convergence of the solutions obtained for the natural frequencies is studied. Also, the present numerical model validated by comparing its numerical results with those reported in literature. Finally, parametric studies are carried out and the effects of a number of important parameters on the natural frequencies are investigated.

Keywords: Free vibration, Piezoelectric, Annular plate, Differential quadrature method

1 Introduction

Application of piezoelectric materials in advanced structures to create in them some kinds of adaptive or "smart" characters has developed over the past few decades. The piezoelectric materials can be used as sensors/actuators in the structural vibration control systems, for measuring the strain and/or exerting the actuation forces on the structure. From structural viewpoint, vibration analysis of piezoelectric coupled circular/annular plates as a structural element in different structural systems, including civil, mechanical, space and marine structures as well as electronic components, has been the subject of many research works. Analytical solution was presented by Wang et al. [1] for vibration analysis of a circular plate surface bonded by two piezoelectric layers, based on the classical plate theory (CPT). Liu et al. [2] proposed an analytical model for free vibration analysis of piezoelectric coupled moderately thick circular plate based on the first-order shear deformation plate theory (FSDT). In their study, a sinusoidal function is adopted to describe the distribution of electric potential along the thickness direction of the piezo patches. By implementing both CPT and FSDT plate theories, analytical solutions were presented by Duan et al. [3] for the free vibrations of piezoelectric coupled annular plate.

[*]Graduate Student, Department of Mechanical Engineering, Karaj Branch, Islamic Azad University, Karaj, Iran
[†] Corresponding Author, Assistant Professor, Department of Mechanical Engineering, Karaj Branch, Islamic Azad University, Karaj – 3148635731, Iran, ghomshei@kiau.ac.ir

They concluded that Mindlin model provides better solutions than those from Kirchhoff model and the error percent of the results is larger for higher resonant frequencies. Wu et. al. [4] investigated vibration behavior of a circular steel substrate surface bonded by a piezoelectric layer with open circuit. In their study, a solution for the electrical potential across piezoelectric layers' thickness was developed for the first time to satisfy the open circuit electrical boundary conditions. Hosseini-Hashemi et al. [5-6] exhibited an exact solution for free vibration analysis of circular/annular moderately thick plates integrated with piezoelectric layers on the basis of the Levinson plate theory (LPT) and third-order shear deformation plate theory (TSDT). Some research works are also devoted to the vibration analysis of piezoelectric coupled circular/annular plates made of functionally graded materials Ebrahimi F and Rastgoo [7]; Hosseini Hashemi et al. [8]; Jafari Mehrabadi et al. [9]; Jodaei et al. [10].

In all the previously mentioned research works analytical solutions are developed for vibration characteristics of the circular/annular plates integrated with piezoelectric layers. Although analytical methods present closed-form solutions, they are limited to simple geometries, specific types of boundary conditions and special loading cases. Differential quadrature method (DQM) is a robust numerical approach which was firstly introduced by Bellman and Casti [11], was applied by Bert et al. [12] for the first time to study dynamic behaviors of structures. There were some limitations in applications of DQ method. For example, the early method for computing the weighting coefficients which was improved by Quan and Chang [13] and, Shu and Richards [14] resulted in ill-conditioned matrices when a large number of grid points are used. Other restrictions, which have limited the application range of the conventional DQ method include restrictions for implementation of multiple boundary conditions when the DQ method is used to solve fourth-order differential equations, discontinuities in geometry and loading, complex structures such as stepped beams under general loadings, and frame structures which led to the introduction of various methods such as δ-technique (Bert et al. [15]; Wang and Bert [16]), equation replaced approach (Shu and Du [17]), quadrature element method (QEM) (Chen [18]; Stritz et al. [19]) and differential quadrature element method (DQEM) (Karami and Malekzadeh [20]; Wang [21]).

In this paper, a numerical solution for free vibration analysis of open circuit piezoelectric coupled is presented by using a combination of differential quadrature (DQ) and generalized differential quadrature (GDQ) methods. The governing differential equations derived according to the Kirchhoff plate theory, and Maxwell equation together with an assumed electric potential function which satisfies the open circuit electrical boundary conditions. These equations are discretized through quadrature rule to convert them as a set of algebraic eigenvalue equations, that can be solved for a number of first natural frequencies and vibration mode shapes of the annular plate. Validation and accuracy of the present DQ solution method are illustrated via comparing its numerical results with those of analytical solutions available in the literature. It is worth noting that, the analytical solutions are confined to some simple or special kinds of boundary conditions, while the present GDQ numerical scheme can be applicable for any kind of plate edge supporting. Applying the GDQ model, parametric studies are conducted to show the influence of various geometrical and material quantities as well as mechanical boundary conditions on the natural frequencies of the piezoelectric coupled annular plates.

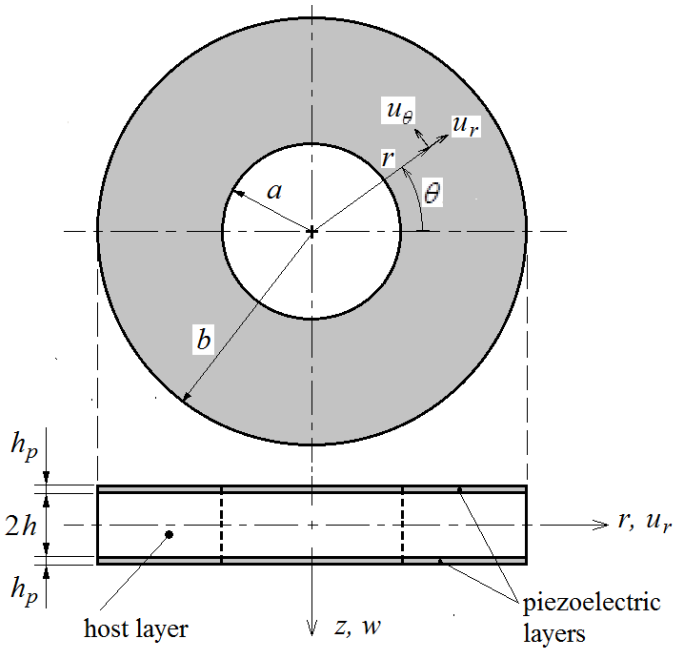

Figure 1 Geometry of a piezoelectric coupled thin annular plate.

2 Mathematical formulation

2.1 Kinematics and constitutive relations

A flat thin piezoelectric coupled annular plate is depicted in Figure (1). The assembly includes a host layer in the middle and two piezoelectric layers which are perfectly bonded to the upper and lower surfaces of the host layer. The inner radius, outer radius, host plate thickness and piezoelectric layer thickness are defined by a, b, $2h$ and h_p, respectively. The top and bottom surfaces of the piezoelectric layers are fully covered by a very tiny electrode material with negligible mechanical effects. The piezoelectric patches are polarized along their thickness direction. In order to extract mathematical formulations, an orthogonal cylindrical coordinate system (r,θ,z) is used with its origin at the mid-surface and its *z* axis coincided with the plate axis of symmetry. For the sake of convenience, superscripts 'h' and 'p' are applied in the formulation to represent the parameters of the host and piezoelectric layers, respectively. According to CPT, the displacement field can be given by [1]:

$$u_z = w(r,\theta,t) \tag{1a}$$

$$u_r = -z\frac{\partial w(r,\theta,t)}{\partial r} \tag{1b}$$

$$u_\theta = -z\frac{\partial w(r,\theta,t)}{r\partial \theta} \tag{1c}$$

where, u_z, u_r and u_θ are the displacements in transverse, *z*, radial, *r*, and tangential, θ, directions, respectively. Also in Eq. (1), *t* represents the past time. Using the displacement field given by Eq. (1) along with small deformation assumption, the following equalities are derived for the strain components ε_{rr}, $\varepsilon_{\theta\theta}$ and $\varepsilon_{r\theta}$ [1]:

$$\varepsilon_{rr} = \frac{\partial u_r}{\partial r} = -z\frac{\partial^2 w}{\partial r^2} \tag{2a}$$

$$\varepsilon_{\theta\theta} = \frac{\partial u_\theta}{r\partial\theta} + \frac{u_r}{r} = -z\left(\frac{\partial^2 w}{r^2\partial\theta^2} + \frac{\partial w}{r\partial r}\right) \tag{2b}$$

$$\varepsilon_{r\theta} = \frac{1}{2}\left(\frac{\partial u_r}{r\partial\theta} + \frac{\partial u_\theta}{\partial r} - \frac{u_\theta}{r}\right) = -z\left(\frac{\partial^2 w}{r\partial r\partial\theta} - \frac{\partial w}{r^2\partial\theta}\right) \tag{2c}$$

According to Hook's law, the stress components in the host plate can be expressed as

$$\sigma_{rr}^{(h)} = \frac{E}{(1-\upsilon^2)}(\varepsilon_{rr} + \upsilon\varepsilon_{\theta\theta}) = -\frac{Ez}{(1-\upsilon^2)}\left[\frac{\partial^2 w}{\partial r^2} + \upsilon\left(\frac{\partial^2 w}{r^2\partial\theta^2} + \frac{\partial w}{r\partial r}\right)\right] \tag{3a}$$

$$\sigma_{\theta\theta}^{(h)} = \frac{E}{(1-\upsilon^2)}(\varepsilon_{\theta\theta} + \upsilon\varepsilon_{rr}) = -\frac{Ez}{(1-\upsilon^2)}\left[\frac{\partial^2 w}{r^2\partial\theta^2} + \frac{\partial w}{r\partial r} + \upsilon\frac{\partial^2 w}{\partial r^2}\right] \tag{3b}$$

$$\tau_{r\theta}^{(h)} = \frac{E}{(1+\upsilon)}\varepsilon_{r\theta} = -\frac{Ez}{(1+\upsilon)}\left[\frac{\partial^2 w}{r\partial r\partial\theta} - \frac{\partial w}{r^2\partial\theta}\right] \tag{3c}$$

in which, υ and E are Poisson's ratio and Young's modulus of the host plate, respectively. In the piezoelectric layer, the constitutive relations can be written as [1]

$$\sigma_{rr}^{(\mathrm{p})} = \bar{C}_{11}^{E}\varepsilon_{rr} + \bar{C}_{12}^{E}\varepsilon_{\theta\theta} - \bar{e}_{31}E_z \tag{4a}$$

$$\sigma_{\theta\theta}^{(\mathrm{p})} = \bar{C}_{12}^{E}\varepsilon_{rr} + \bar{C}_{11}^{E}\varepsilon_{\theta\theta} - \bar{e}_{31}E_z \tag{4b}$$

$$\tau_{r\theta}^{(\mathrm{p})} = (\bar{C}_{11}^{E} - \bar{C}_{12}^{E})\varepsilon_{r\theta} \tag{4c}$$

where,

$$\bar{C}_{11}^{E} = C_{11}^{E} - \frac{(C_{13}^{E})^2}{C_{33}^{E}} \tag{5a}$$

$$\bar{C}_{12}^{E} = C_{12}^{E} - \frac{(C_{13}^{E})^2}{C_{33}^{E}} \tag{5b}$$

$$\bar{e}_{31} = e_{31} - \frac{C_{13}^{E}e_{33}}{C_{33}^{E}} \tag{5c}$$

in those, C_{11}^{p}, C_{12}^{p}, C_{13}^{p} and C_{33}^{p} are the moduli of elasticity under constant electric field, and e_{31}, e_{33} are the piezoelectric constants. Also, E_r, E_θ, and E_z are the electric field intensities in the radial, tangential and transverse directions respectively, which can be obtained by the derivatives of the electric potential field, ϕ, as below [1]

$$E_r = -\frac{\partial\phi}{\partial r} \tag{6a}$$

$$E_\theta = -\frac{\partial\phi}{r\partial\theta} \tag{6b}$$

$$E_z = -\frac{\partial\phi}{\partial z} \tag{6c}$$

and, their corresponding electric displacements D_r, D_θ and D_z are derived by [1]:

$$D_r = \Xi_{11}E_r \tag{7a}$$

$$D_\theta = \Xi_{11}E_\theta \tag{7b}$$

$$D_z = \bar{e}_{31}(\varepsilon_{rr} + \varepsilon_{\theta\theta}) + \bar{\bar{\Xi}}_{33} E_z \tag{7c}$$

where,

$$\bar{\bar{\Xi}}_{33} = \Xi_{33} + \frac{e_{33}^2}{C_{33}^E} \tag{8}$$

in that, Ξ_{11} and Ξ_{33} are the dielectric constants of the piezoelectric layer.

2.2 Electric potential distribution in piezoelectric layers

For the open circuit piezoelectric layer, an electric potential function proposed by Wu et. al. [4], which satisfies the open circuit electrical boundary condition, is used herein which can be defined by:

$$\phi = \left\{1 - \left[\frac{2z - (H+h)}{H-h}\right]^2\right\}\varphi(r,\theta,t) + Az + B, \;\; H = h + h_p \tag{9}$$

where, *A* and *B* are two parameter as functions of r, θ and z which can be determined by applying the electrical boundary condition for open circuit piezoelectric layer, and $\varphi(r,\theta,t)$ is the electric potential on the mid-surface of the piezoelectric layer. Since each piezoelectric patch is surface bonded on one side of the metal host plate, the electric potential on their interface is null, so,

$$\phi(z = h) = 0 \tag{10}$$

and, the electric displacement at the free surfaces of piezoelectric patches almost vanish as the surfaces are completely isolated [4], that is,

$$D_z(z = H) = 0 \tag{11}$$

Applying the boundary conditions given by Eq. (10) and Eq. (11), the functions *A* and *B* can be obtained as follows:

$$A = -\frac{B}{h} = \frac{4}{h_p}\varphi - \frac{H\bar{e}_{31}}{\bar{\bar{\Xi}}_{33}}\Delta w \tag{12}$$

where , Δ is the Laplace operator in polar coordinate system and is given by

$$\Delta = \frac{\partial^2}{\partial r^2} + \frac{\partial}{r\partial r} + \frac{\partial^2}{r^2\partial\theta^2} \tag{13}$$

Thus, the electric potential function can be written as

$$\phi = -\frac{4(z-h)(z-2H+h)}{(H-h)^2}\varphi - \frac{\bar{e}_{31}}{\bar{\bar{\Xi}}_{33}} H(z-h)\Delta w \tag{14}$$

Eq. (14) gives the electric distribution function along the thickness direction of the open circuit piezoelectric layer. Substituting Eq. (14) into Eq. (6), yields three components of the electric field

$$E_r = 4\frac{(z-h)(z-2H+h)}{(H-h)^2}\frac{\partial\varphi}{\partial r} + \frac{\bar{e}_{31}}{\bar{\bar{\Xi}}_{33}}\mathrm{H}(z-h)\frac{\partial(\Delta w)}{\partial r} \tag{15a}$$

$$E_\theta = 4\frac{(z-h)(z-2H+h)}{(H-h)^2}\frac{\partial\varphi}{r\partial\theta} + \frac{\bar{e}_{31}}{\bar{\bar{\Xi}}_{33}}\mathrm{H}(z-h)\frac{\partial(\Delta w)}{r\partial\theta} \tag{15b}$$

$$E_z = 8\frac{z-H}{(H-h)^2}\varphi + \frac{\bar{e}_{31}}{\bar{\bar{\Xi}}_{33}}\mathrm{H}\,\Delta w \tag{15c}$$

and, the corresponding electric displacements are derived as the following:

$$D_r = 4\Xi_{11}\frac{(z-h)(z-2H+h)}{(H-h)^2}\frac{\partial\varphi}{\partial r} + \frac{\Xi_{11}\bar{e}_{31}}{\bar{\Xi}_{33}}\mathrm{H}(z-h)\frac{\partial(\Delta w)}{\partial r} \tag{16a}$$

$$D_\theta = 4\Xi_{11}\frac{(z-h)(z-2H+h)}{(H-h)^2}\frac{\partial\varphi}{r\partial\theta} + \frac{\Xi_{11}\bar{e}_{31}}{\bar{\Xi}_{33}}\mathrm{H}(z-h)\frac{\partial(\Delta w)}{r\partial\theta} \tag{16b}$$

$$D_z = 8\bar{\Xi}_{33}\frac{z-H}{(H-h)^2}\varphi - \bar{e}_{31}(z-H)\Delta w \tag{16c}$$

Also, the stress components in a piezoelectric layer given by Eq. (4) can be rewritten as:

$$\sigma_{rr}^{(p)} = -\left(\bar{C}_{11}^E z + H\frac{\bar{e}_{31}^{\,2}}{\bar{\Xi}_{33}}\right)\frac{\partial^2 w}{\partial r^2} - \left(\bar{C}_{12}^E z + H\frac{\bar{e}_{31}^{\,2}}{\bar{\Xi}_{33}}\right)\left(\frac{\partial^2 w}{r^2\partial\theta^2} + \frac{\partial w}{r\partial r}\right) - 8\bar{e}_{31}\frac{z-H}{(H-h)^2}\varphi \tag{17a}$$

$$\sigma_{\theta\theta}^{(p)} = -\left(\bar{C}_{12}^E z + H\frac{\bar{e}_{31}^{\,2}}{\bar{\Xi}_{33}}\right)\frac{\partial^2 w}{\partial r^2} - \left(\bar{C}_{11}^E z + H\frac{\bar{e}_{31}^{\,2}}{\bar{\Xi}_{33}}\right)\left(\frac{\partial^2 w}{r^2\partial\theta^2} + \frac{\partial w}{r\partial r}\right) - 8\bar{e}_{31}\frac{z-H}{(H-h)^2}\varphi \tag{17b}$$

$$\tau_{r\theta}^{(p)} = -(\bar{C}_{11}^E - \bar{C}_{12}^E)z\left(\frac{\partial^2 w}{r\partial r\partial\theta} - \frac{\partial w}{r^2\partial\theta}\right) \tag{17c}$$

2.3 Motion and Maxwell equations with respective B.C.'s

The expression for bending moments M_{rr}, $M_{\theta\theta}$ and twisting moment $M_{r\theta}$ are

$$M_{rr} = \int_{-H}^{H} z\sigma_{rr}dz = \int_{-h}^{h} z\sigma_{rr}^{(h)}dz + 2\int_{h}^{H} z\sigma_{rr}^{(p)}dz \tag{18a}$$

$$M_{\theta\theta} = \int_{-H}^{H} z\sigma_{\theta\theta}dz = \int_{-h}^{h} z\sigma_{\theta\theta}^{(h)}dz + 2\int_{h}^{H} z\sigma_{\theta\theta}^{(p)}dz \tag{18b}$$

$$M_{r\theta} = \int_{-H}^{H} z\tau_{r\theta}dz = \int_{-h}^{h} z\tau_{r\theta}^{(h)}dz + 2\int_{h}^{H} z\tau_{r\theta}^{(p)}dz \tag{18c}$$

Substituting Eqs. (3) and Eqs. (17) into the Eqs. (18), leads to the following expressions for the resultant moments

$$M_{rr} = A_1\frac{\partial^2 w}{\partial r^2} + A_2\left(\frac{\partial^2 w}{r^2\partial\theta^2} + \frac{\partial w}{r\partial r}\right) + A_3\varphi \tag{19a}$$

$$M_{\theta\theta} = A_2\frac{\partial^2 w}{\partial r^2} + A_1\left(\frac{\partial^2 w}{r^2\partial\theta^2} + \frac{\partial w}{r\partial r}\right) + A_3\varphi \tag{19b}$$

$$M_{r\theta} = (A_1 - A_2)\left(\frac{\partial^2 w}{r\partial r\partial\theta} - \frac{\partial w}{r^2\partial\theta}\right) \tag{19c}$$

where,

$$A_1 = -\frac{2Eh^3}{3(1-\upsilon^2)} - \frac{2(H^3-h^3)\bar{C}_{11}^E}{3} - \frac{H(H^2-h^2)(\bar{\mathrm{e}}_{31})^2}{\bar{\Xi}_{33}} \tag{20a}$$

$$A_2 = -\frac{2E\upsilon h^3}{3(1-\upsilon^2)} - \frac{2(H^3-h^3)\bar{C}_{12}^E}{3} - \frac{H(H^2-h^2)(\bar{\mathrm{e}}_{31})^2}{\bar{\Xi}_{33}} \tag{20b}$$

$$A_3 = \frac{8}{3}(H+2h)\,\bar{e}_{31} \tag{20c}$$

The resultant shearing forces q_r and q_θ can be obtained by [4]:

$$q_r = \frac{\partial M_{rr}}{\partial r} + \frac{\partial M_{r\theta}}{r\partial\theta} + \frac{M_{rr} - M_{\theta\theta}}{r} \tag{21a}$$

$$q_\theta = \frac{\partial M_{r\theta}}{\partial r} + \frac{\partial M_{\theta\theta}}{r\partial\theta} + \frac{2M_{r\theta}}{r} \tag{21b}$$

Also, by substituting Eqs. (19) into Eqs. (21), the following expressions for the shearing forces are derived

$$q_r = A_1 \frac{\partial}{\partial r}(\Delta \mathrm{w}) + A_3 \frac{\partial \varphi}{\partial r} \tag{22a}$$

$$q_\theta = A_1 \frac{\partial}{r\partial\theta}(\Delta \mathrm{w}) + A_3 \frac{\partial \varphi}{r\partial\theta} \tag{22b}$$

Now, according to the Kirchhoff plate model, the equation of motion along *z* axis expressed for an element of the laminated plate in cylindrical coordinate, is given by [4]

$$\frac{\partial q_r}{\partial r} + \frac{\partial q_\theta}{r\partial\theta} + \frac{q_r}{r} = \int_{-h}^{h} \rho^{(h)} \frac{\partial^2 w}{\partial t^2} dz + 2\int_{h}^{H} \rho^{(p)} \frac{\partial^2 w}{\partial t^2} dz \tag{23}$$

where, ρ^h and ρ^p are the density of the host plate and the piezoelectric layers, respectively. Substitution of Eqs. (22) into Eq. (23), yields the governing equation of vibrations for the smart laminated plate based on the CPT

$$A_1 \Delta\Delta w + A_3 \Delta\varphi + \bar{\rho} \frac{\partial^2 w}{\partial t^2} = 0 \tag{24}$$

where,

$$\bar{\rho} = 2\left[\rho^{(h)} h + \rho^{(p)}(H-h)\right] \tag{25}$$

The Maxwell equation, integrated over the piezoelectric layer thickness, say the lower one, may be expressed as below [3]

$$\int_{h}^{H} \left[\frac{\partial (rD_r)}{r\partial r} + \frac{\partial D_\theta}{r\partial\theta} + \frac{\partial D_z}{\partial z} \right] dz = 0 \tag{26}$$

This states that integration over the thickness from the divergence of the electric flux vanishes. Now, by substituting from Eq. (16) into Eq. (26), we reach to the following PDE

$$B_1 \Delta\Delta w + B_2 \Delta\varphi + B_3 \Delta w + B_4 \varphi = 0 \tag{27}$$

in that,

$$B_1 = \frac{H(H-h)\,\bar{e}_{31}\,\Xi_{11}}{2\bar{\Xi}_{33}} \tag{28a}$$

$$B_2 = -\frac{8(H-h)\Xi_{11}}{3} \tag{28b}$$

$$B_3 = -(H-h)\,\bar{e}_{31} \tag{28c}$$

$$B_4 = \frac{8\bar{\Xi}_{33}}{H-h} \tag{28d}$$

For a thin annular plate, the expressions for clamped and simply-supported boundary conditions, which may be applied on the inner and/or outer edge of the annular plate, are given as follows

At a clamped edge:

$$w = 0, \qquad \frac{\partial w}{\partial r} = 0 \tag{29}$$

At a simply-supported edge:

$$w = 0, \qquad M_{rr} = 0 \tag{30}$$

If the plate is insulated at the edge, the electrical flux conservation equation is given by [3],

$$\int_{h}^{H} D_r(\mathrm{r},\theta,\mathrm{t})\,\mathrm{dz} = 0 \tag{31}$$

Substituting from Eq. (16a) into the above equation, the electric boundary condition is obtained as:

$$\frac{\partial \varphi}{\partial r} = 0 \tag{32}$$

The solutions for $w(r,\theta,\mathrm{t})$ and $\varphi(r,\theta,t)$ can be considered as below [3]:

$$w(r,\theta,t) = W(r)e^{i(p\theta-\omega t)} \tag{33}$$

$$\varphi(r,\theta,t) = \Psi(r)e^{i(p\theta-\omega t)} \tag{34}$$

where, $W(r)$ and $\Psi(r)$ are the amplitude of the displacement and electric potential in the plate thickness direction as functions of only the r coordinate, ω is the natural frequency of vibrations, and p is the wave number in θ direction. Now, substitution of Eqs. (33) and (34) into Eqs. (24) and (27), yields

$$A_1\overline{\Delta\Delta}W + A_3\bar{\Delta}\Psi = \bar{\rho}\omega^2 W \tag{35}$$

$$B_1\overline{\Delta\Delta}W + B_2\bar{\Delta}\Psi + B_3\bar{\Delta}W + B_4\Psi = 0 \tag{36}$$

where,

$$\bar{\Delta} = \frac{d^2}{dr^2} + \frac{1}{r}\frac{d}{dr} - \frac{k^2}{r^2} \tag{37}$$

$$\overline{\Delta\Delta} = \frac{d^4}{dr^4} + \frac{2}{r}\frac{d^3}{dr^3} - \frac{2k^2+1}{r^2}\frac{d^2}{dr^2} + \frac{2k^2+1}{r^3}\frac{d}{dr} + \frac{k^4-4k^2}{r^4} \tag{38}$$

in those k is the same as p, i.e. the wave number in θ direction ($k = p$). Also, the mechanical and electrical boundary conditions can be rewritten in terms of W and Ψ as below:

Mechanical B.C's. at a clamped edge:

$$W = 0, \quad \frac{dW}{dr} = 0 \tag{39}$$

Mechanical B.C's. at a simply-supported edge:

$$W = 0,$$
$$A_1\frac{d^2W}{dr^2} + A_2\frac{1}{r}\frac{dW}{dr} - A_2\frac{k^2}{r^2}W + A_3\Psi = 0 \tag{40}$$

Electrical B.Cs. for piezo patches:

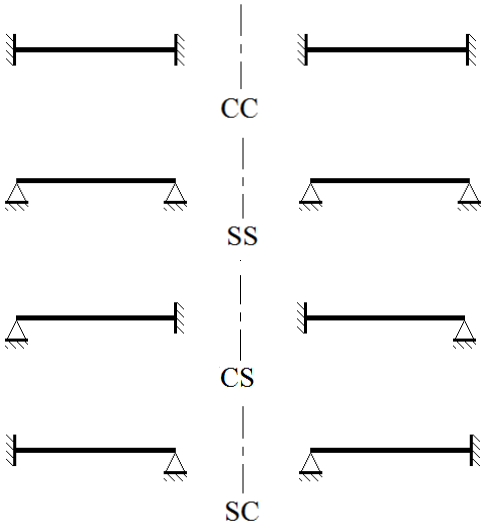

Figure 2 Four types of supporting applied on the piezoelectric coupled annular plate, CC, SS, CS and SC respectively.

$$\frac{d\Psi}{dr} = 0 \tag{41}$$

To obtain the annular plate natural frequencies and corresponding mode shapes, two forth order ordinary differential equations given by Eqs. (35), (36) should be solved regarding one of the edge supporting conditions given by Eqs. (39)- (41) applied to the inner ($r = a$) and/or outer ($r = b$) circular boundaries of the annular plate. In the present work four different combinations of mechanical boundary conditions applied at the two circular edges are considered namely, Clamed–Clamed (CC), Simple–Simple (SS), Simple–Clamped (SC) and Clamed–Simple (CS), where the first and second letter denote the boundary condition at the inner and outer edge, respectively.
In Figure (2) each of the four types of supporting are shown schematically.

3 Problem solution

3.1 Review of differential quadrature method

In differential quadrature method, an n*th*-order x-partial derivative of function $f(x)$ at a grid point $x = x_i$ may be approximated as [22]:

$$\frac{d^n f(x_i)}{dx^n} = \sum_{j=1}^{N} A_{ij}^{(n)} f(x_j), \qquad i = 1,2,...,N, \;\; n = 1,2,...,N-1 \tag{42}$$

where N is the number of grid points and $A_{ij}^{(n)}$ are the weighting coefficients for calculating the n*th*-order derivative at the i^{th} sampling point. The procedure adopted for determination of the weighting coefficients and the quality of selection of the grid points in the solution domain, are two the key points in the successful application of the differential quadrature method. In this paper, we adopted the procedure introduced by Shu and Richards [14] which has been demonstrated to make more accurate computational results than the other methods. According to their rule, the weighting coefficients of the first-order derivatives with respect to a spatial variable say *x*, can be determined as [22]

$$A_{ij}^{(1)}=\begin{cases}\dfrac{M(x_i)}{(x_i-x_j)M(x_j)}, & \text{for} \quad i\neq j\\ -\sum\limits_{j=1,i\neq j}^{N}A_{ij}^{(1)}, & \text{for} \quad i=j\end{cases} \quad ; \quad i,j=1,2,3,...,N \tag{43}$$

where,

$$M(x_i)=\prod_{k=1,\mathrm{i}\neq\mathrm{k}}^{N}(x_i-x_k) \tag{44}$$

and, the weighting coefficients of second, third, and fourth-order derivatives, $A_{ij}^{(2)}$, $A_{ij}^{(3)}$ and $A_{ij}^{(4)}$, may be computed by

$$A_{ij}^{(2)}=\sum_{k=1}^{N}A_{ik}^{(1)}A_{kj}^{(1)} \tag{45}$$

$$A_{ij}^{(3)}=\sum_{k=1}^{N}A_{ik}^{(1)}A_{kj}^{(2)} \tag{46}$$

$$A_{ij}^{(4)}=\sum_{k=1}^{N}A_{ik}^{(1)}A_{kj}^{(3)} \tag{47}$$

Also, in Shu and Richards procedure an unequally spaced grid point distribution so-called Chebyshev nodes is applied, which can be expressed in a domain $x\in[a\ \ b]$ as [14]

$$x_k=a+\frac{b-a}{2}\left[1-\cos\left(\pi\frac{k-1}{N-1}\right)\right], \quad k=1,2,...,N \tag{48}$$

3.2 Generalized differential quadrature rule

The essence of GDQR (generalized differential quadrature rule) and differential quadrature element method (DQEM) is based on applying two degrees of freedoms (DOFs) at the end points, namely, w_1, $w_1^{(1)}$, w_N, $w_N^{(1)}$, instead of one DOF to handle the two boundary conditions. The weighting coefficients of the first-order derivatives in GDQR based on the Lagrange interpolation can be modified by [23]:

$$E_{ij}^{(1)}=\begin{cases}A_{ij}^{(1)} & \text{for} \quad i=1,2,...,N;\ \ j=1,2,...,N\\ 0 & \text{for} \quad i=1,2,...,N;\ \ j=N+1,N+2\end{cases} \tag{49}$$

The weighting coefficients of the second-order derivatives for all inner grid points $(i=2,3,...,N-1)$ can be determined by [23]

$$E_{ij}^{(2)}=\begin{cases}A_{ij}^{(2)} & \text{for} \quad i=2,3,...,N-1,\ \ j=1,2,...,N\\ 0 & \text{for} \quad i=2,3,...,N-1,\ \ j=N+1,N+2\end{cases} \tag{50}$$

and at the two end points (i.e. $i=1,N$) are computed differently as follows,

$$\begin{aligned}&E_{ij}^{(2)}=\sum_{k=2}^{N-1}A_{ik}^{(1)}A_{kj}^{(1)} \quad \text{for} \quad j=1,2,...,N,\\ &E_{i(N+1)}^{(2)}=A_{i1}^{(1)}, \quad E_{i(N+2)}^{(2)}=A_{iN}^{(1)}\end{aligned} \tag{51}$$

Eq. (51) is derived regarding the fact that the second-order derivative with respect to x at the two end points can be computed by using the DQ rule, namely,

$$f_i''=\sum_{k=1}^{N}\bar{A}_{ik}f_k'=\sum_{k=2}^{N-1}\bar{A}_{ik}f'+\bar{A}_{i1}f_1'+\bar{A}_{iN}f_N'$$
$$=\sum_{k=2}^{N-1}\bar{A}_{ik}\sum_{j=1}^{N}\bar{A}_{kj}f_j+\bar{A}_{i1}f_1'+\bar{A}_{iN}f_N'=\sum_{j=1}^{N+2}B_{ij}\delta_j;\quad i=1,N \tag{52}$$

The obvious difference between Eq. (52) and Eq. (42) rewritten for n=2, is that in the former the range of summation changes from 1 to N + 2. The weighting coefficients of the third- and fourth-order derivatives with respect to x can simply be computed by [23]

$$E_{ij}^{(3)}=\sum_{k=1}^{N}A_{ik}^{(1)}E_{kj}^{(2)};\quad i=1,2,...,N,\quad j=1,2,...,N+2 \tag{53}$$

$$E_{ij}^{(4)}=\sum_{k=1}^{N}A_{ik}^{(2)}E_{kj}^{(2)};\quad i=1,2,...,N,\quad j=1,2,...,N+2 \tag{54}$$

3.3 Discretization of the differential equations by DQM and GDQR

In this section, the two governing differential equations (35), (36) of the piezoelectric coupled annular plate are transformed into algebraic equations by implementing the GDQR and DQM respectively, along with their associated boundary conditions. This is because there are two mechanical B.Cs. at each boundary point, while there is only one electrical B.C. at each edge point.

First, substituting from Eqs. (37) and (38) into the Eqs. (35) and (36), the two forth-order governing differential equations can be rewritten as the following expanded forms:

$$A_1\frac{d^4W}{dr^4}+A_1\frac{2}{r}\frac{d^3W}{dr^3}-A_1\frac{2k^2+1}{r^2}\frac{d^2W}{dr^2}+A_1\frac{2k^2+1}{r^3}\frac{dW}{dr}$$
$$+A_1\frac{k^4-4k^2}{r^4}W+A_3\frac{d^2\Psi}{dr^2}+A_3\frac{1}{r}\frac{d\Psi}{dr}-A_3\frac{k^2}{r^2}\Psi=\omega^2\bar{\rho}W \tag{55}$$

$$B_1\frac{d^4W}{dr^4}+B_1\frac{2}{r}\frac{d^3W}{dr^3}+\left(B_3-B_1\frac{2k^2+1}{r^2}\right)\frac{d^2W}{dr^2}+\left(B_1\frac{2k^2+1}{r^3}+B_3\frac{1}{r}\right)\frac{dW}{dr}$$
$$+\left(B_1\frac{k^4-4k^2}{r^4}-B_3\frac{k^2}{r^2}\right)W+B_2\frac{d^2\Psi}{dr^2}+B_2\frac{1}{r}\frac{d\Psi}{dr}+\left(B_4-B_2\frac{k^2}{r^2}\right)\Psi=0 \tag{56}$$

Now, by implementing the GDQR and DQM respectively to Eq. (55) and (56), with the weighting coefficients $A_{ij}^{(n)}$ and $E_{ij}^{(n)}$ previously determined as described in sections 3.1 and 3.2, the discrete form of the equations are obtained as

$$\sum_{j=1}^{N+2}\left[A_1E_{ij}^{(4)}+\frac{2A_1}{r_i}E_{ij}^{(3)}-\frac{(2k^2+1)A_1}{r_i^2}E_{ij}^{(2)}+\frac{(2k^2+1)A_1}{r_i^3}E_{ij}^{(1)}\right]W_j$$
$$+\frac{(k^4-4k^2)A_1}{r_i^4}W_i+\sum_{j=1}^{N}\left[A_3A_{ij}^{(2)}+\frac{A_3}{r_i}A_{ij}^{(1)}\right]\Psi_j-A_3\frac{k^2}{r_i^2}\Psi_i$$
$$=\omega^2\bar{\rho}W_i\quad(i=2,3,...,N-1) \tag{57}$$

$$\sum_{j=1}^{N+2}\left[B_1 E_{ij}^{(4)} + \frac{2B_1}{r_i} E_{ij}^{(3)} + \left(B_3 - B_1 \frac{2k^2+1}{r_i^2} \right) E_{ij}^{(2)} + + \left(B_1 \frac{2k^2+1}{r_i^3} + B_3 \frac{1}{r_i} \right) E_{ij}^{(1)} \right] W_j$$
$$+ \left(B_1 \frac{k^4 - 4k^2}{r_i^4} - B_3 \frac{k^2}{r_i^2} \right) W_i + \sum_{j=1}^{N}\left[B_2 A_{ij}^{(2)} + \frac{B_2}{r_i} A_{ij}^{(1)} \right] \Psi_j + \left(B_4 - B_2 \frac{k^2}{r_i^2} \right) \Psi_i$$
$$= 0 \quad (i = 2,3,...,N-1) \tag{58}$$

The discretized form of the boundary condition, e.g. for an annular plate having SC edge supporting, can be considered as

$$W_1 = \sum_{j=1}^{N+2}\left[A_1 E_{1j}^{(2)} + \frac{A_2}{a} E_{1j}^{(1)} \right] W_j - \frac{k^2 A_2}{a^2} W_1 + A_3 \Psi_1 = 0 \tag{59a}$$

$$W_N = W_N^{(1)} = 0 \tag{59b}$$

Also, the electrical boundary condition given in Eq. (41) can be discretized as

$$\sum_{j=1}^{N} A_{1j}^{(1)} \Psi_j = \sum_{j=1}^{N} A_{Nj}^{(1)} \Psi_j = 0 \tag{60}$$

Assembling the discrete forms of the governing equations given in Eqs. (57)-(58), then applying the discretized boundary equations (59), (60), yields a set of $(2N+2)\times(2N+2)$ algebraic equations which can be written in the matrix form as an eigenvalue problem given by

$$\left([K] - \omega^2 [M] \right) [X] = 0 \tag{61}$$

where, $[K]$ and $[M]$ are the stiffness and mass matrices, respectively, and $[X]$ is the eigen vector or the vector of node point variables defined as

$$[X] = \begin{Bmatrix} U \\ \Psi \end{Bmatrix}, \quad [U] = \begin{Bmatrix} W_1 \\ W_2 \\ . \\ . \\ . \\ W_N \\ W_1^{(1)} \\ W_N^{(1)} \end{Bmatrix}, \quad [\Psi] = \begin{Bmatrix} \Psi_1 \\ \Psi_2 \\ . \\ . \\ . \\ \Psi_N \end{Bmatrix} \tag{62}$$

By solving the eigenvalue equation, Eq. (61), the natural frequencies and mode shapes of the plate lateral vibrations can be determined.

4 Results and discussions

A computer code in MATLAB is developed to solve the eigenvalue equation given by Eq. (61). In these computations the material and geometrical properties are as listed in Table (1), unless otherwise specified. For convenience, the notation ω_{pn} is used to represent a natural frequency corresponding to the mode number (p, n), in that p and n denote the number of nodal diameters and nodal circles respectively. It should be mentioned that the number of nodal diameters and nodal circles are defined as the number of zeros in the θ-direction and in the r-direction respectively which are counted in their whole domains [3].

Table 1 Material and geometrical properties of the host and piezoelectric layers [3].

Property	Host layer (Steel)	Piezoelectric layer (PZT4)
Young's moduli (N/m^2)	$E = 200\times10^9$	$C_{11}^E = 132\times10^9$
	-	$C_{12}^E = 71\times10^9$
	-	$C_{13}^E = 73\times10^9$
	-	$C_{33}^E = 115\times10^9$
	-	
Mass density (kg/m^3)	$\rho^h = 7.8\times10^3$	$\rho^p = 7.5\times10^3$
e_{31} (C/m^2)	-	-4.1
e_{33} (C/m^2)	-	14.1
Ξ_{11} (F/m)	-	7.124×10^{-9}
Ξ_{33} (F/m)	-	5.841×10^{-9}
a (m)	0.1	0.1
b (m)	0.6	0.6
h (m)	0.01	-
h_p (m)	-	0.001

4.1 Convergence and comparative studies

In this section, the convergence of the present numerical solution is investigated with increasing the number of node points for a set of mode shapes corresponding to $p = 0,1,2$ and $n = 0,1,2$, computed for two different types of the edge supporting conditions CC and SS. Figure (3) shows the convergence patterns of the plate natural frequencies for all combinations of these mode numbers and supporting conditions.
Regarding these diagrams, it is found that:

● Irrespective to the plate supporting type, the natural frequencies of the sandwich plate converge to a stable value as the number of grid points increases. It can be observed that considering a number of grid points *N*=27, often makes sufficiently accurate results for the natural frequencies ω_{pn} with *n* and *p* up to 2.

● For various mode numbers (*p*, *n*), different convergence rates may be observed. However, the convergence rate for the modes of the smallest number of nodal diameters (i.e. $p = 0$) is faster than those of $p = 1,2$.

● For all of the mode numbers, the plate boundary conditions play an important role in the convergence rate of the GDQM. It may be seen that the convergence rate for the plate of SS supporting type is faster than that of the plate of CC supporting type.

In order to verify the accuracy and capability of the present GDQM, natural frequencies of a piezoelectric coupled annular plates of various boundary conditions including CC, SS, SC and CS, have been obtained for three different values of nodal circles ($n = 0,1,2$) and nodal diameters ($p = 0,1,2$). The numerical data have been achieved by $N = 35$ grid points and are tabulated in Table (2).

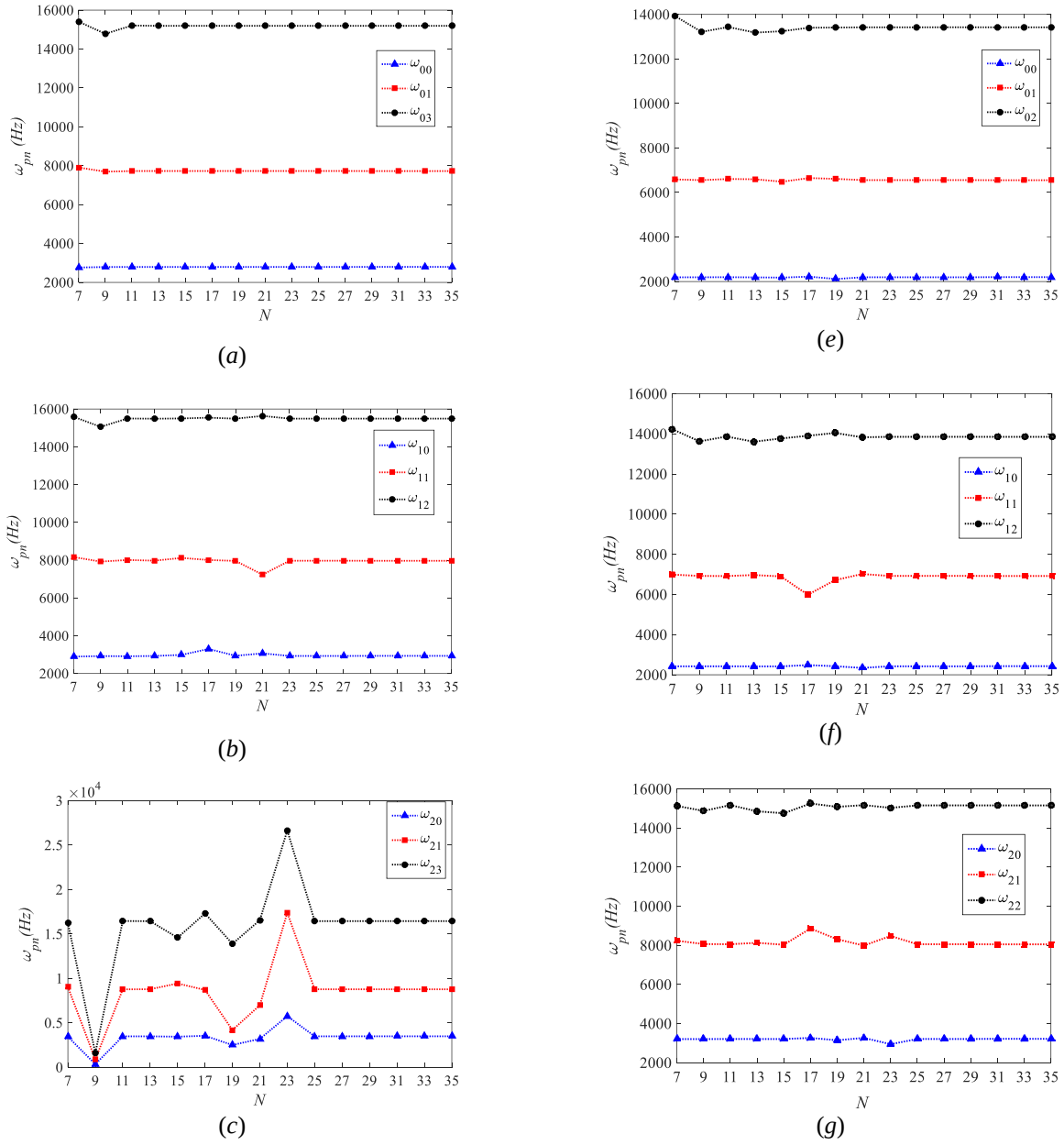

Figure 3 Convergence of the first three natural frequencies ($n = 0,1,2$) of the piezoelectric coupled annular plate versus the number of grid points, a) CC, $p = 0$; b) CC, $p = 1$ c) CC, $p = 2$; e) SS, $p = 0$; f) SS, $p = 1$; g) SS, $p = 2$

In this table the results of the exact solutions performed by Duan et al. [3] and those from 3D FE analyses by ABAQUS 6.3 [3] are also included for comparison. According to the tabulated results, it may clearly be seen that the numerical results of the present GDQM are very close to those of the exact and the FEM solutions reported in the reference (Duan et al. [3]). Therefore, it can be concluded that the present GDQM provides an accurate and reliable numerical solution formulation. Furthermore, by comparing the percentage differences given in Table (2), it is observed that at the higher modes of vibration (modes with greater nodal circles) the difference is more significant. Corresponding to the tabulated natural frequencies, the vibration mode shapes of the annular plates are shown in Figure (4) just for CC and SS types of boundary conditions.

Table 2 Comparison of natural frequencies (rad/s) of piezoelectric coupled annular plates with different boundary conditions for h/a=.1.

Boundary Condition	p	n	Present GDQM	Exact (Duan et al. [3])	Diff. %	FEM (Duan et al. [3])	Diff. %
CC	0	0	2797.48	2815	0.62	2812	0.52
		1	7725.01	7786	0.78	7659	-0.86
		2	15192.16	15306	0.74	14753	-2.98
	1	0	2934.31	2952	0.60	2942	0.26
		1	7967.12	8030	0.78	7882	-1.08
		2	15492.16	15608	0.74	15020	-3.14
	2	0	3483.88	3506	0.63	3471	-0.37
		1	8772.34	8840	0.77	8635	-1.59
		2	16445.89	16569	0.74	15877	-3.58
SS	0	0	1386.84	1396	0.66	1395	0.58
		1	5159.67	5198	0.74	5173	0.26
		2	11394.39	11489	0.82	11283	-0.99
	1	0	1604.06	1613	0.55	1593	-0.69
		1	5522.76	5558	0.63	5490	-0.60
		2	11821.95	11918	0.81	11647	-1.50
	2	0	2341.76	2355	0.56	2312	-1.29
		1	6613.92	6669	0.82	6521	-1.42
		2	13150.19	13225	0.57	12798	-2.75
CS	0	0	1832.22	1843	0.58	1848	0.85
		1	6190.89	6220	0.47	6164	-0.44
		2	13013.64	13111	0.74	12770	-1.91
	1	0	1971.77	1983	0.57	1981	0.47
		1	6428.74	6459	0.47	6384	-0.70
		2	13311.91	13411	0.74	13038	-2.10
	2	0	2518.77	2535	0.64	2511	-0.31
		1	7206.40	7259	0.72	7134	-1.01
		2	14262.50	14367	0.73	13903	-2.59
SC	0	0	2197.97	2216	0.81	2213	0.68
		1	6552.76	6615	0.94	6544	-0.13
		2	13420.94	13531	0.81	13169	-1.91
	1	0	2428.72	2446	0.71	2418	-0.44
		1	6919.57	6983	0.91	6865	-0.79
		2	13848.46	13961	0.81	13528	-2.37
	2	0	3216.69	3236	0.60	3178	-1.22
		1	8051.14	8119	0.84	7902	-1.89
		2	15154.08	15274	0.79	14663	-3.35

4.2 Parametric studies

In the previous subsection the convergence and accuracy of the developed generalized differential quadrature formulation has been investigated and verified. In this subsection, by implementing the present GDQM, the effects of a number of geometrical and material parameters as well as mechanical boundary conditions on the natural frequencies of the piezoelectric coupled annular plates are examined. All the numerical data presented hereafter have been achieved by N=35 grid points.

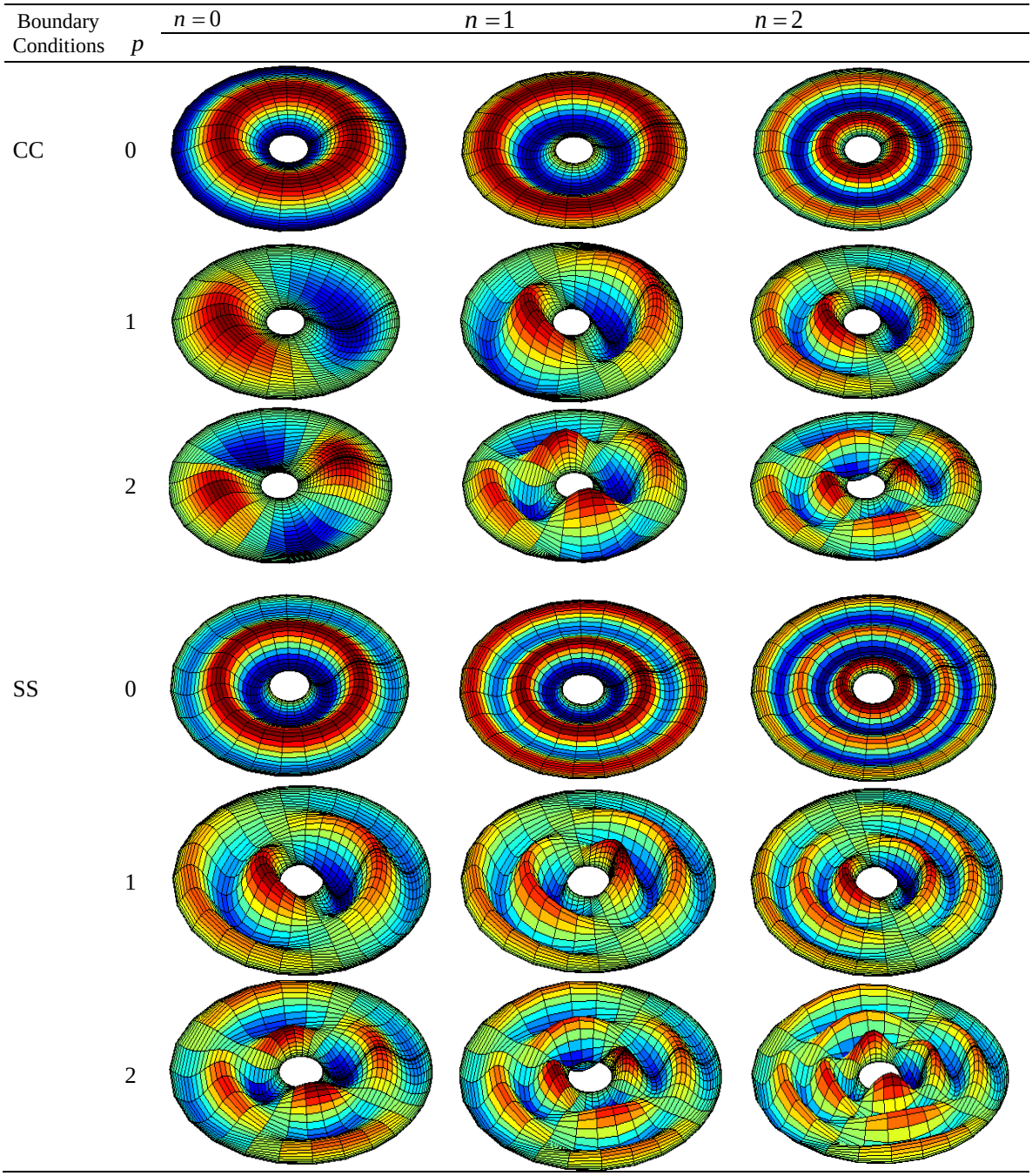

Figure 4 Lateral vibration mode shapes of the piezoelectric coupled annular plates with CC and SS Boundary conditions for h/a=0.1.

In Figures (5), (6) effect of the outer/inner radius ratio (b/a) on the natural frequency is investigated. The variations of the first three natural frequencies ω_{00}, ω_{01}, ω_{02} of the piezoelectric coupled annular plate as functions of the outer/inner radius ratio (b/a) have been depicted in Figures (5), (6) respectively for CC and SC edge conditions. The outer radius, b, is varied from 0.2 to 1m in steps of 0.1 m, while the inner radius is maintained constant value a=0.1 m.

It may be found that by increasing b/a, all the natural frequencies in the logarithmic scale are decreased almost with the same attitude.

Figure (7) shows three first natural frequencies ω_{00}, ω_{01}, ω_{02} of the SS smart annular plate versus the host plate thickness to inner radius ratio (h/a). The host plate thickness takes the values

$h = 5,6,7,8,9,10$ mm while the inner radius is maintained a constant value a=0.1 m, and the thickness of the piezoelectric layers is assumed to be 10% of the host plate thickness. As may be observed in Figure (7), the natural frequencies, expressed in the logarithmic scale, increase smoothly as h/a takes larger values. Figure (8) depicts the variation in the natural frequencies of the CC smart annular plate versus the piezoelectric to host thickness ratio (h_p / h) for $n = 0,1,2$ and nodal diameter number $p = 1$. The host plate thickness is assumed to be of constant value $h = 0.01$m, while the thickness of the piezoelectric layers varies from 0.0005 to 0.004 m in steps of 0.0005 m.

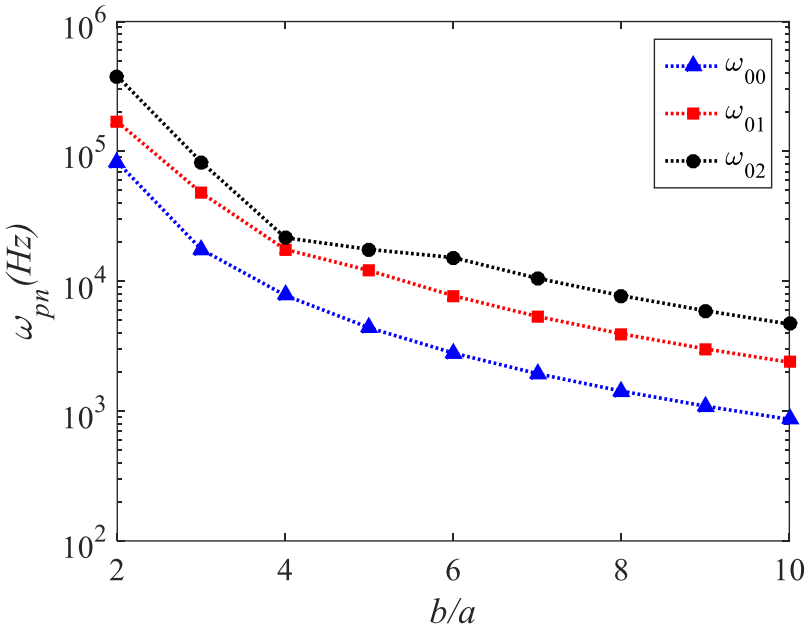

Figure 5 Variation of the first three natural frequencies of the piezoelectric coupled annular plate versus the outer/inner radius ratio, *b/a*, (CC, *h/a*=0.1, $a = 0.1$m, $n = 0,1,2$, $p = 0$)

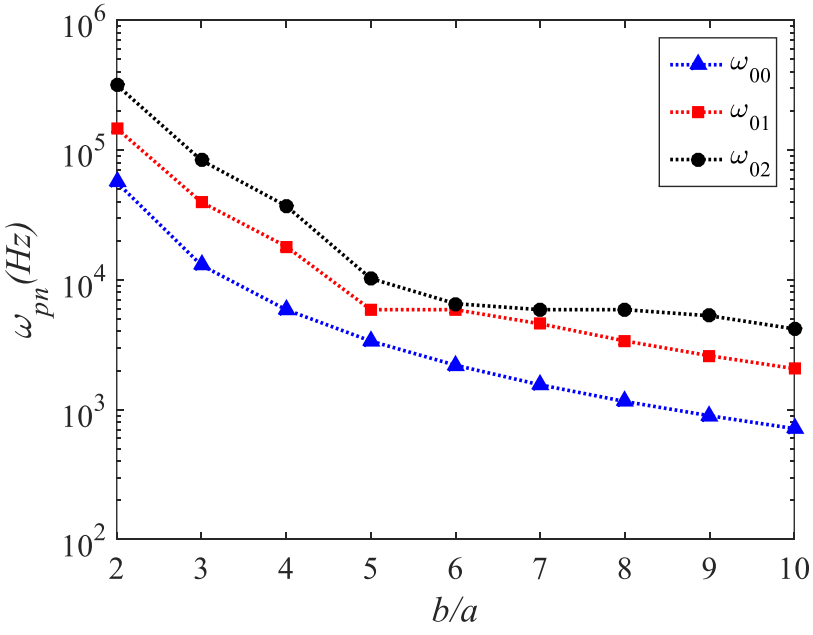

Figure 6 Variation of the first three natural frequencies of the piezoelectric coupled annular plate versus the outer/inner radius ratio, *b/a*, (SC, *h/a*=0.1, $a = 0.1$m, $n = 0,1,2$, $p = 0$)

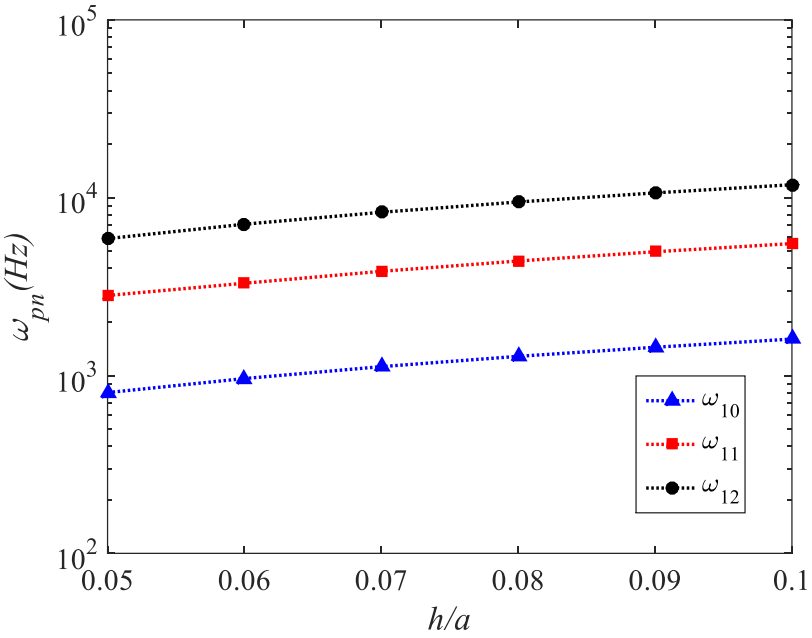

Figure 7 Variation of the first three natural frequencies of the piezoelectric coupled annular plate versus the host plate thickness to inner radius ratio, *h/a*, (SS, *b*/*a*=6, $a = 0.1\text{m}$, $n = 0,1,2$, $p = 1$)

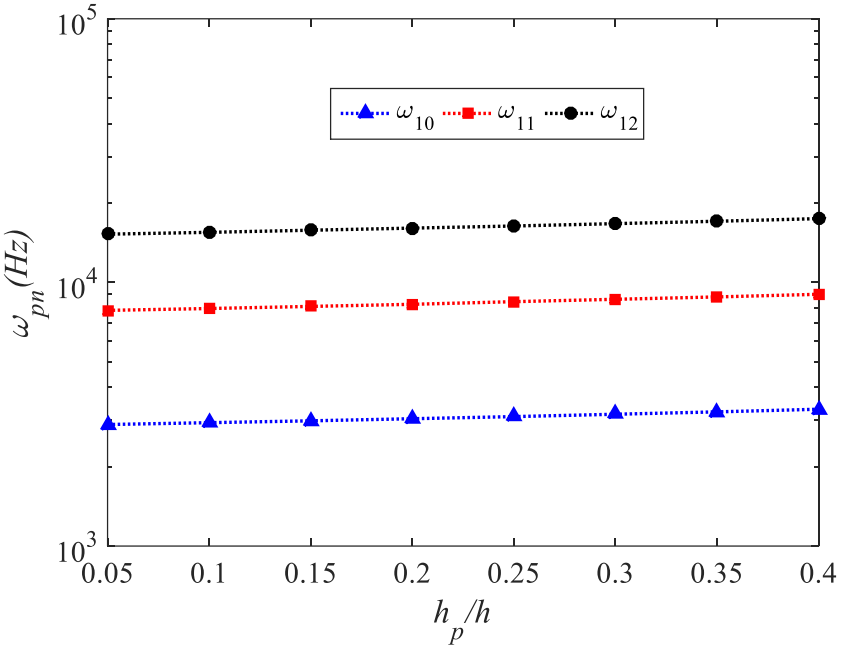

Figure 8 Variation of the first three natural frequencies of the piezoelectric coupled annular plate with the piezoelectric to host thickness ratio (CC, *h*/*a*=0.1, *h*=0.01 m, $n = 0,1,2$, $p = 1$)

From this figure which illustrates the effect of the piezoelectric patches, it can be realized that the natural frequencies in the logarithmic scale rise almost linearly as the piezoelectric to host thickness ratio (h_p / h) increases.

In Figure (9) the annular plate natural frequency ω_{p0} is plotted versus the nodal diameter number, *p*, for 4 different types of boundary conditions. It may be observed that higher restraining boundary conditions such as CC and SC, cause larger natural frequencies in the plate. However, the increasing effect of the supporting type on the amount of the natural frequency diminishes for higher nodal diameter numbers. Comparison between the curves of

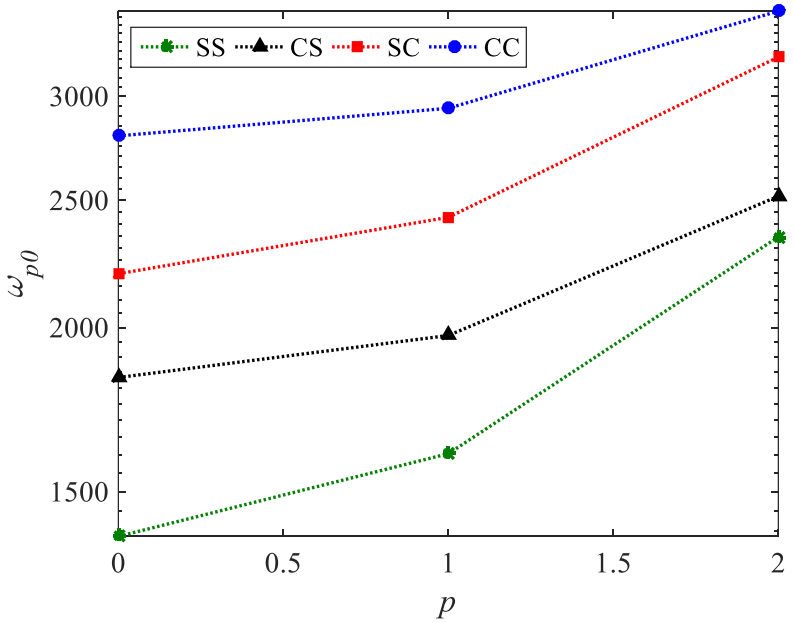

Figure 9 Natural frequency ω_{p0} of the piezoelectric coupled annular plate versus nodal diameter number, p, for various boundary conditions (b/a=6, h/a=0.1).

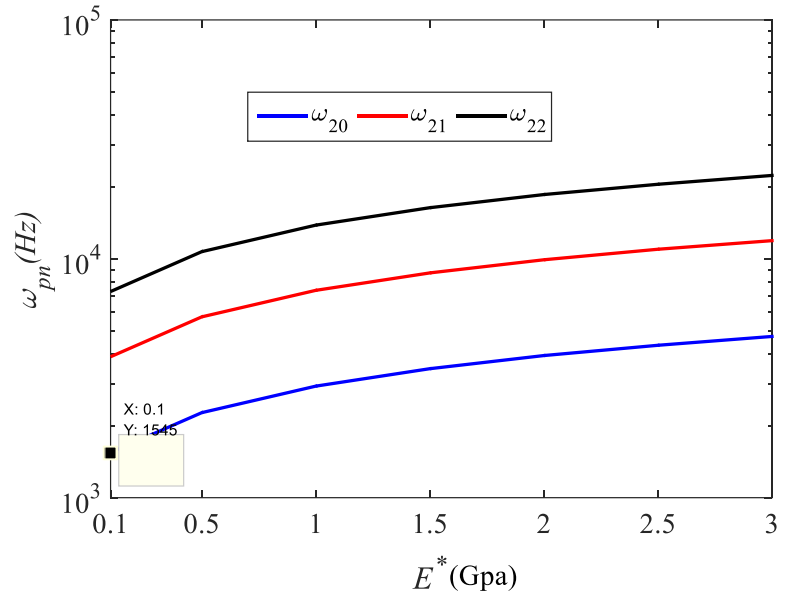

Figure 10 Variation of the first three natural frequencies of the piezoelectric coupled annular plate with the host to piezoelectric modulus ratio, E^*, (CC, b/a=6, h/a=0.1. $p=2$, $n=0,1,2$).

CS and SC shows that the frequencies of SC are greater than those of CS, which may be explained by the fact that clamping the outer edge causes more rise in the plate stiffness than doing the inner edge.

Denoting the ratio of the host plate modulus to piezoelectric modulus as E^*, the variation of three natural frequencies ω_{20}, ω_{21}, ω_{22} of the CC smart annular plate with E^* has been illustrated in Figure (10) ($0.1 \le E^* = E/C_{11}^E \le 3$). For this purpose, while all other parameters are kept fixed, the host plate modulus varied in the range $10 < E < 400$ GPa.

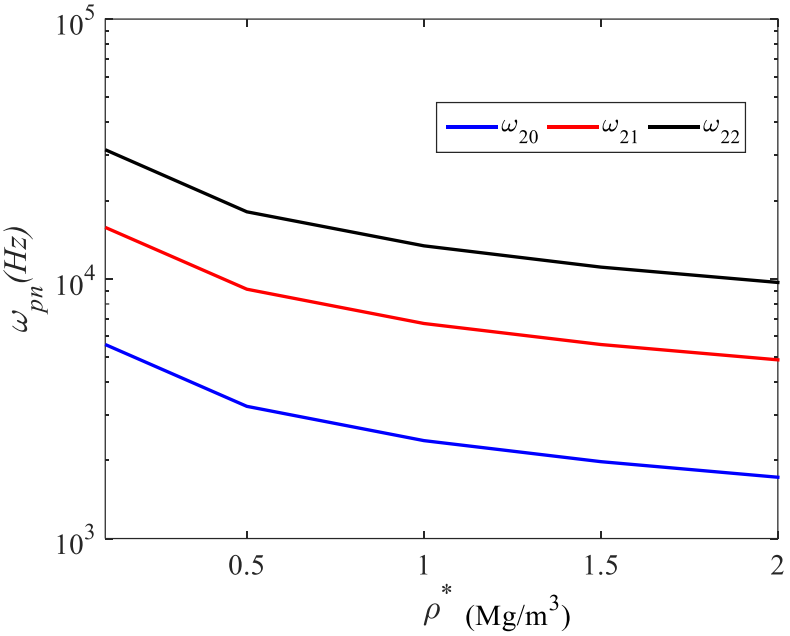

Figure 11 Variation of the first three natural frequencies ($n = 0,1,2$) of the piezoelectric coupled annular plate versus the host plate to piezoelectric density ratio, ρ^*, (SS, *b*/*a*=6, *h*/*a*=0.1. $p = 2$).

It can be inferred from this figure that as E^* takes larger values, the natural frequencies increase. Figure (11) provides information about the change in the first three natural frequencies of the SS smart annular plate as the host plate to piezoelectric density ratio, $\rho^* = \rho^h / \rho^p$, varies in the range $0.1 < \rho^* < 2$, while keeping all other parameters fixed, for $n = 0,1,2$ and $p = 2$. It can be inferred from this figure that the natural frequencies decline as the host plate to piezoelectric density ratio, ρ^*, increases.

5 Concluding remarks

In the present research work, a numerical solution formulation is proposed for small amplitude free vibrations of the open circuit piezoelectric coupled thin annular plates using the generalized differential quadrature method (GDQM). The convergence studies were carried out to determine the number of grid points required for an accurate solution of the problem.
It was found that to achieve a converged solution for the natural frequencies, the number of grid points should be increased for larger mode numbers. The accuracy and validity of the present GDQ formulation are verified through comparative studies. Moreover, implementing the present GDQ numerical scheme, the effects of geometrical and material parameters as well as mechanical boundary conditions on the natural frequencies are studied in detail and the following conclusions are extracted:

By increasing the outer to inner radius ratio, *b/a*, while the inner radius is maintained constant, all the natural frequencies are decreased almost with the same attitude. The natural frequencies, expressed in the logarithmic scale, increase smoothly as the host plate thickness to inner radius ratio, h/a, takes larger values.
Similarly, the logarithm of the natural frequencies rise almost linearly as the piezoelectric to host thickness ratio (h_p / h) increases. Also, it is observed that higher restraining boundary conditions such as CC and SC, cause larger natural frequencies in the plate. However, the raising effect of the supporting type on the amount of the natural frequency diminishes for

higher nodal diameter numbers. Furthermore, as the host plate modulus to piezoelectric modulus ratio, E^*, takes larger values, the natural frequencies increase. However, as the host plate density to piezoelectric density ratio, ρ^*, increases, the natural frequencies are declined.

References

[1] Wang, Q., Quek, S.T., Sun, C.T., and Liu, X., "Analysis of Piezoelectric Coupled Circular Plate", Smart Materials and Structures, Vol. 10, pp. 229-39, (2001).

[2] Liu, X., Wang, Q., and Quek, S.T., "Analytical Solution for Free Vibration of Piezoelectric Coupled Moderately Thick Circular Plates", International Journal of Solids and Structures, Vol. 39, pp. 2129–2151, (2002).

[3] Duan, W.H., Quek, S.T., and Wang, Q., "Free Vibration Analysis of Piezoelectric Coupled Thin and Thick Annular Plate", Journal of Sound and Vibration, Vol. 281, pp. 119–39, (2005).

[4] Wu, N., Wang, Q., and Quek, S.T., "Free Vibration Analysis of Piezoelectric Coupled Circular Plate with Open Circuit", Journal of Sound and Vibration, Vol. 329, pp. 1126–1136, (2010).

[5] Hosseini-Hashemi, Sh., Es'haghi, M., and Karimi, M., "Closed-form Solution for Free Vibration of Piezoelectric Coupled Annular Plates using Levinson Plate Theory", Journal of Sound and Vibration, Vol. 329, pp. 1390–1408, (2010).

[6] Hosseini Hashemi, Sh., Es'haghi, M., and Rokni Damavandi Taher, H., "An Exact Analytical Solution for Freely Vibrating Piezoelectric Coupled Circular/Annular Thick Plates using Reddy Plate Theory", Composite Structures, Vol. 92, pp. 1333-1351, (2010).

[7] Ebrahimi, F., and Rastgoo, A., "Free Vibration Analysis of Smart Annular FGM Plates Integrated with Piezoelectric Layers", Smart Materials and Structures, Vol. 17, pp. 15-24, (2008).

[8] Hosseini Hashemi, Sh., Es'haghi, M., and Karimi, M., "Closed-form Vibration Analysis of Thick Annular Functionally Graded Plates with Integrated Piezoelectric Layers", International Journal of Mechanical Science, Vol. 52, pp. 410-428, (2010).

[9] Jafari Mehrabadi, S., Kargarnovin, M.H., and Najafizadeh, M.M., "Free Vibration Analysis of Functionally Graded Coupled Circular Plate with Piezoelectric Layers", Journal of Mechanical Science and Technology, Vol. 23, pp. 2008-2021, (2009).

[10] Jodaei, A., Jalal, M., and Yas, M.H., "Three-dimensional Free Vibration Analysis of Functionally Graded Piezoelectric Annular Plates via SSDQM and Comparative Modeling by ANN", Mathematical and Computer Modeling, Vol. 57, pp. 1408-1425, (2013).

[11] Bellman, R.E., and Casti, J., "Differential Quadrature and Long-term Integration", Journal of Mathematical Analysis and Applications, Vol. 34, pp. 235–238, (1971).

[12] Bert, C.W., Wang, X., and Striz, A.G., "Differential Quadrature for Static and Free Vibration Analyses of Anisotropic Plates", International Journal of Solids and Structures, Vol. 30, No. 13, pp. 1737–1744, (1993).

[13] Quan, J.R., and Chang, C.T., "New Insights in Solving Distributed System Equations by the Quadrature Method - I. Analysis", Computers and Chemical Engineering, Vol. 13, pp. 779-788, (1989).

[14] Shu, C., and Richards, B.E., "Application of Generalized Differential Quadrature to Solve Two-dimensional Incompressible Navier-Strokes Equations", International Journal for Numerical Methods in Fluids, Vol. 15, pp. 791-798, (1992).

[15] Bert, C.W., Jang, S.K., and Striz, A.G., "Two New Approximate Methods for Analyzing Free Vibration of Structural Components", AIAA Journal, Vol. 26, pp. 612–618, (1988).

[16] Wang, X., and Bert, C.W., "A New Approach in Applying Differential Quadrature to Static and Free Vibrational Analyses of Beams and Plates", Journal of Sound and Vibration Vol. 162, No. 3, pp. 566–572, (1993).

[17] Shu, C., and Du, H., "A Generalized Approach for Implementing General Boundary Conditions in the GDQ Free Vibration Analysis of Plates", International Journal of Solids and Structures, Vol. 34, No. 7, pp. 837-846, (1997).

[18] Chen, W., "A New Approach for Structural Mechanics: The Quadrature Element Method", PhD Thesis, Department of Mechanical Engineering, University of Oklahoma, Oklahoma, USA, (1994).

[19] Stritz, A.G., Chen, W., and Bert, C.W., "Static Analysis of Structures by the Quadrature Element Method (QEM)", International Journal of Solids and Structures Vol. 31, No. 20, pp. 2807–2818, (1994).

[20] Karami, G., and Malekzadeh, P., "A New Differential Quadrature Methodology for Beam Analysis and the Associated Differential Quadrature Element Method", Computer Methods in Applied Mechanics and Engineering, Vol. 191, pp. 3509-3526, (2002).

[21] Wang, X., Tan, M., and Zhou, Y., "Buckling Analyses of Anisotropic Plates and Isotropic Skew Plates by the new Version Differential Quadrature Method", Thin-Walled Structures, Vol. 41, pp. 15–29, (2003).

[22] Wang, X., Liu, F., and Gan, L., "New Approaches in Application of Differential Quadrature Method for Fourth-order Differential Equations", Communications in Numerical Methods in Engineering, Vol. 21, No. 2, Vol. 61–71, (2005).

[23] Wang, X., "*Differential Quadrature and Differential Quadrature Based Element Methods; Theory and Applications*", Elsevier Incorporated, USA, (2015).

Nomenclatures

a	Inner radius
b	Outer radius
$C_{11}^{p}, C_{12}^{p}, C_{13}^{p}, C_{33}^{p}$	Piezoelectric moduli of elasticity under constant electric field
D_r, D_θ, D_z	Components of the electric displacements
E	Young modulus of the host plate
E_r, E_θ, E_z	Components of the electric field intensity
e_{31}, e_{33}	Piezoelectric constants
h	One-half of the host plate thickness
h_p	Piezoelectric layer thickness
$[K]$	Mass matrix
$[M]$	Stiffness matrix
$M_{rr}, M_{\theta\theta}, M_{r\theta}$	Bending and twisting moments
p	Wave number in θ direction
q_r, q_θ	Resultant shearing forces
(r,θ,z)	Coordinates of the cylindrical coordinate system
u_r	Radial displacement
u_θ	Displacement along θ coordinate
u_z	Displacement along z coordinate
$W(r)$	Amplitude of the transverse displacement
$[X]$	Eigen vector or the vector of node point variables
$\varepsilon_{rr}, \varepsilon_{\theta\theta}, \varepsilon_{r\theta}$	Strain components
Ξ_{11}, Ξ_{33}	Dielectric constants of the piezoelectric layer
ρ^h, ρ^p	Mass density of the host and piezoelectric layers resp.
$\sigma_{rr}^{(h)}, \tau_{r\theta}^{(h)}, \sigma_{\theta\theta}^{(h)}$	Stress components in the host layer
$\sigma_{rr}^{(p)}, \tau_{r\theta}^{(p)}, \sigma_{\theta\theta}^{(p)}$	Stress components in the piezoelectric layers
υ	Poisson's ratio of the host plate
ϕ	Electric potential field
$\Psi(r)$	Amplitude of the electric potential
ω	Natural frequency of vibrations
$()^{(h)}$	Superscripts *h* refers to the host layer
$()^{(p)}$	Superscripts *p* refers to the piezoelectric layers